Analysis of Trapped Image Guides Using Effective Dielectric Constant and Surface Impedances

WEN-BIAO ZHOU AND TATSUO ITOH, FELLOW, IEEE

Abstract—**A method has been introduced to accurately predict dispersion characteristics of the trapped image guide. Numerical results agreed much better with experimental results than those previously calculated by a simple effective dielectric constant (EDC) approach especially at the low frequency end.**

I. Introduction

IT IS WELL known that reduction of the radiation loss at curved sections, junctions, and discontinuities is important in a millimeter-wave integrated circuit based on dielectric waveguides. The trapped image guide proposed recently has a potential to reduce the radiation loss at curved sections [1]. This waveguide consists of a dielectric rod placed in a metal trough as shown in Fig. 1(a). It was confirmed that the radiation loss at a horizontal bend is much less than in the case of a conventional image guide. In [1], the analysis was carried out by neglecting the fields in regions 5 and 6 in Fig. 1(a) and subsequently applying the effective dielectric constant (EDC) method. The results of such an analysis are not accurate at low frequencies where the effect of fields in regions 5 and 6 becomes more important.

This paper presents a new method of analysis which predicts the characteristics of the trapped image guide much more accurately especially at low frequencies. Comparison of the numerical results with experimental data confirms the usefulness of this new method.

II. Analysis Procedure

Since the trapped image guide is a modification of the image guide, the modal fields in the former are expected to resemble those in the latter especially at higher frequencies. Therefore, we classify the guided modes into E^y- and E^x-types. In the E^y modes, the predominant field components are E_y and H_x, whereas in the E^x modes E_x and H_y are dominant. In this paper, we consider only the dominant E^y mode, as this is the most important in practice.

The strategy is to first find an equivalent structure Fig. 1(c) of the original one in Fig. 1(a) by way of an intermediate structure in Fig. 1(b). We then apply the transverse resonance condition at the dielectric–air interface

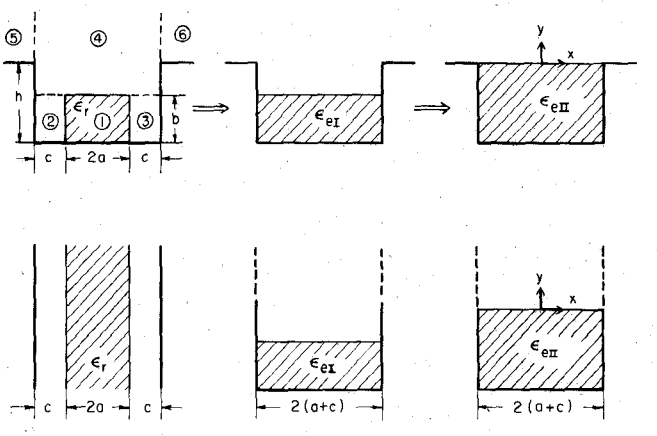

Fig. 1. Cross section of the trapped image guide and its equivalent structures.

$y = 0$ in Fig. 1(c) after the effect of the free space $y > 0$, $|x| < \infty$ is taken into account.

The first step is to use the effective dielectric constant (EDC) method to obtain the intermediate structure Fig. 1(b). The EDC of the area consisting of regions 1, 2, and 3 can be obtained by solving the eigenvalue problem of Fig. 1(d) in which an infinitely long dielectric slab is sandwiched between two infinitely long vertical metal walls by way of air regions of width c. This is a two-dimensional structure for which an exact formulation is readily derived by matching E_y and H_z at $x = \pm a$. The eigenvalue equation for the transverse wavenumber k_x in the slab is

$$\xi \cosh(\xi c)\cos(k_x a) - k_x \sinh(\xi c)\sin(k_x a) = 0 \quad (1)$$

where

$$\xi = \left[(\epsilon_r - 1)k_0^2 - k_x^2\right]^{1/2} \quad (2)$$

and k_0 is the free-space wavenumber. Once (1) is solved for k_x, the EDC of the area made of regions 1, 2, and 3 is given by

$$\epsilon_{eI} = \epsilon_r - \left(\frac{k_x}{k_0}\right)^2. \quad (3)$$

The EDC is thought of as the dielectric constant of a hypothetical medium in which the phase velocity of a plane wave is identical to that of a guided wave in the two-dimensional structure Fig. 1(d). The area made of regions 1, 2, and 3 is now replaced with this EDC ϵ_{eI} as shown in Fig. 1(b).

Manuscript received March 16, 1982; revised June 9, 1982. This work was supported in part by the U.S. Army Research Office under Contract DAAG29-81-K-0053.

The authors are with the Department of Electrical Engineering, University of Texas, Austin, TX 78712.

0018-9480/82/1200-2163$00.75 ©1982 IEEE

The next step is to transform the hypothetical structure in Fig. 1(b) to still another equivalent structure in Fig. 1(c) in which the new effective dielectric constant ϵ_{eII} fills the trough up to the height h. The value of ϵ_{eII} may be obtained in the following manner. We consider the structures in Fig. 1(e) and Fig. 1(f) which are obtained by extending the height of side walls in Fig. 1(b) and 1(c) to infinity. If the modal field is well guided, the propagation constant in Fig. 1(e) is very close to the one in Fig. 1(b) and similarly the ones in Fig. 1(f) and Fig. 1(c) are close. We choose ϵ_{eII} in such a way that the propagation constant β in the z direction in Fig. 1(f) is identical to the one in Fig. 1(e). To this end, we proceed as follows.

The field in Fig. 1(e) is given by a scalar potential

$$\phi = \begin{Bmatrix} Ae^{-\bar{v}y} \\ B\cos \bar{u}(y+h) \end{Bmatrix} \cdot \cos\left[\frac{n\pi x}{2(a+c)}\right] \quad \begin{matrix} y > -(h-b) \\ -h < y < -(h-b) \end{matrix}. \tag{4}$$

The eigenvalue equation for the transverse wavenumber $\bar{u}$ is obtained by matching the tangential fields at $y = -(h-b)$

$$\bar{u} \tan \bar{u}b = \epsilon_{eI}\bar{v} \tag{5}$$

$$\beta^2 + \left[\frac{n\pi}{2(a+c)}\right]^2 = \epsilon_{eI}k_0^2 - \bar{u}^2 = k_0^2 + \bar{v}^2. \tag{6}$$

Similarly, the characteristic equation for the transverse wavenumber u in ϵ_{eII} is

$$u \tan uh = \epsilon_{eII} v \tag{7}$$

$$\beta^2 + \left[\frac{n\pi}{2(a+c)}\right]^2 = \epsilon_{eII}k_0^2 - u^2 = k_0^2 + v^2. \tag{8}$$

Since β's for two structures are assumed identical, v and $\bar{v}$ must be equal. We compare (6) and (8), and (5) and (7), respectively, to obtain

$$\epsilon_{eII} = \frac{\epsilon_{eI}k_0^2 + u^2 - \bar{u}^2}{k_0^2} \tag{9}$$

$$\frac{u \tan uh}{\epsilon_{eI}k_0^2 + u^2 - \bar{u}^2} = \frac{\bar{u} \tan \bar{u}b}{\epsilon_{eI}k_0^2}. \tag{10}$$

In summary, we solve (5) and (6) for $\bar{u}$ using ϵ_{eI} obtained in the previous step, solve (10) for u using the value of $\bar{u}$ just obtained and finally calculate ϵ_{eII} from (9). This ϵ_{eII} is now used to fill the trough completely as shown in Fig. 1(c).

The final step is to impose the transverse resonance condition at $y = 0$ so that the effect of free space $y > 0$ including regions 5 and 6 is taken into account, though in an approximate manner. The technique we will employ has previously been developed by Kaneki in conjunction with a channel waveguide for surface wave antenna application[2]. We will follow his method except for necessary changes.

We apply the transverse resonance condition $\vec{Z}_a + \overleftarrow{Z}_\epsilon = 0$ at $y = 0$ in Fig. 1(c), where $\vec{Z}_a$ is the impedance looking into air at $y = 0$, $|x| < \infty$ and $\overleftarrow{Z}_\epsilon$ that of ϵ_{eII} medium at $y = 0$, $|x| < a + c$. The former can be derived by computing the reactive power P_a per unit length in z, penetrating into air from the dielectric surface $y = 0$

$$P_a = \frac{1}{2\pi}\int_{-\infty}^{\infty} \left[\bar{E}_z\bar{H}_x^* - \bar{E}_x\bar{H}_z^*\right] dk_x \tag{11}$$

where $\bar{E}_z$, $\bar{H}_x$, etc., are Fourier transforms of surface field components

$$\begin{matrix} \bar{E}_{x,z} \\ \bar{H}_{x,z} \end{matrix} = \int_{-\infty}^{\infty} \begin{matrix} E_{x,z}(x,0,z) \\ H_{x,z}(x,0,z) \end{matrix} e^{-jk}x^x dx. \tag{12}$$

We now assume that the field in ϵ_{eII} in Fig. 1(c) is very close to the one in ϵ_{eII} in Fig. 1(f). Under this assumption, all the field components needed for (11) can be derived from the scalar potential

$$\phi = Q\cos u(y+h)\cos\left[\frac{\pi x}{2(a+c)}\right] \tag{13}$$

for the dominant mode. Using these field components, we obtain

$$P_a = -\pi\omega\epsilon_0\left[\frac{Qu}{\epsilon_{eII}(a+c)}\right]^2 J(\beta)\cdot\sin^2(uh) \tag{14}$$

where ω is the angular frequency and $J(\beta)$ is a function of unknown β and can be calculated quite efficiently as shown in the Appendix. The impedance $\vec{Z}_a$ is given by

$$\vec{Z}_a = P_a/|\mathrm{I}|^2 \tag{15}$$

where I is the mode current in the y direction due to the magnetic field at the dielectric surface $y = 0$.

To obtain $\overleftarrow{Z}_\epsilon$, we compute the power P_ϵ per unit length in the z direction, transported from the interface $y = 0$ into the dielectric region ϵ_{eII}

$$P_\epsilon = 2j\omega(\overline{W}_m - \overline{W}_e) \tag{16}$$

where $\overline{W}_e$ and $\overline{W}_m$ are the average electric and magnetic energy, respectively, and are given by

$$\begin{matrix} \overline{W}_e \\ \overline{W}_m \end{matrix} = \frac{1}{2}\int_{-h}^{0}\int_{-(a+c)}^{(a+c)} \begin{matrix} \epsilon_0\epsilon_{eII}|\bar{E}|^2 \\ \mu_0|H|^2 \end{matrix} dx\,dy. \tag{17}$$

Hence, P_ϵ is given by

$$P_\epsilon = jQ^2\frac{\omega\epsilon_0(a+c)u}{2\epsilon_{eII}}\left[\beta^2 + \frac{\pi^2}{4(a+c)^2}\right]\sin 2uh \tag{18}$$

and

$$\overleftarrow{Z}_\epsilon = P_\epsilon/|I|^2. \tag{19}$$

The transverse resonance condition $\vec{Z}_a + \overleftarrow{Z}_\epsilon = 0$ becomes

$$\epsilon_{eII}(a+c)\left[\beta^2 + \frac{(\pi/2)^2}{(a+c)^2}\right]\sin^2 uh - \left[\frac{2\pi u}{(a+c)^2}\right]|J(\beta)|\sin^2 uh = 0. \tag{20}$$

The propagation constant of the original trapped image guide is assumed to be given by the solution of (20).

III. Numerical and Experimental Results

Some numerical results are presented in Fig. 2 along with experimental data for the E_{11}^y mode of three trapped image guides with identical dielectric rods but with differ-

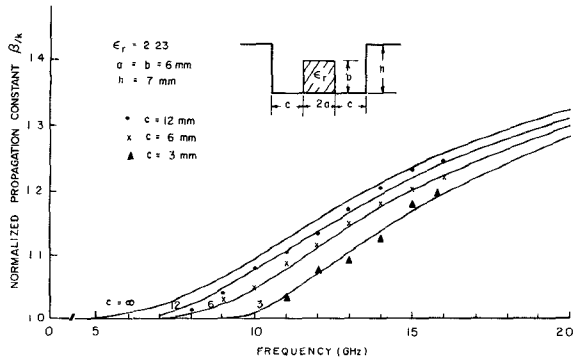

Fig. 2. Theoretical and experimental dispersion characteristics.

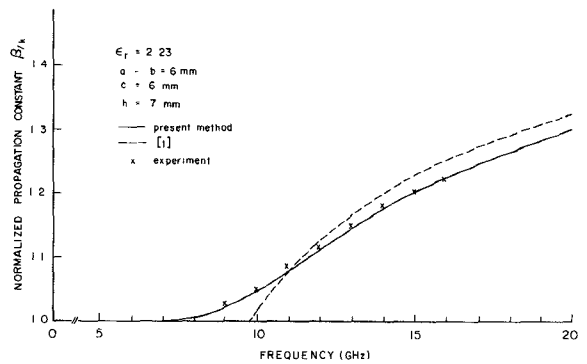

Fig. 3. Comparison between the present method and [1].

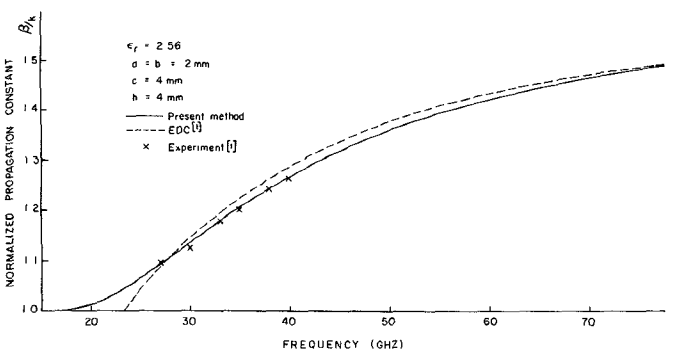

Fig. 4. Comparison between the present method and [1].

ent sidewall spacings. For comparison, the characteristics of the conventional image guide ($c = \infty$) with the same rod dimensions are included. It is seen that the effect of the sidewalls are more pronounced for smaller spacing c of the sidewalls. We also performed an experimental measurement of the propagation constant by means of a movable probe [3] between 8 and 16 GHz and plotted in Fig. 2 with •, x, and Δ. It is clear that agreement between theoretical and experimental results is quite good even at lower frequencies. This was not the case in [1] in which a conventional EDC method was used after the fields in regions 5 and 6 in Fig. 1(a) were neglected.

Comparison between the present method and the previous EDC theory is given in Figs. 3 and 4. It is evident that the present method provides much more accurate results especially at lower frequencies. In fact, the previous method cannot correctly predict the dispersion characteristics at lower frequencies because the field in regions 5 and 6 is

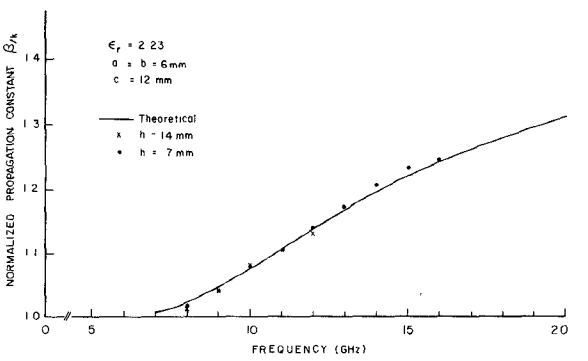

Fig. 5. Effect of height of sidewalls on the dispersion characteristics.

neglected. On the other hand, such a field is incorporated in the solution process in the new method. Experimental results in Fig. 3 are obtained by the movable probe while those in Fig. 4 are reproduced from the previous work [1]. Fig. 4 indicates that the results by both methods agree well at higher frequencies.

Fig. 5 studies the effect of the sidewall height h on the propagation constant. Both theoretical and experimental studies indicate little difference in results due to differences in h as long as h is reasonably larger than b. In fact, it was not possible to distinguish theoretical results on the figure.

This result is surprising because we expect that the effect of fields in regions 5 and 6 is stronger for a smaller value of h. We conjecture the reason for this phenomenon as follows. The most important contribution to the present analysis is the aperture field at $y = 0$, $|x| < a + c$. This contribution is more accurately incorporated in this study than in the previous one. The field in regions 5 and 6 may be of second-order importance. This is strictly a supposition and more extensive investigations need to be done by using different materials and dimensions.

IV. Conclusions

The method presented here is found to provide numerical dispersion characteristics much more accurate than the one previously available for the trapped image guide structure. The method is based on the effective dielectric constant and the transverse resonance of an equivalent structure. The method is more useful in the design of the trapped image guide.

Appendix
Evaluation of $J(\beta)$

From (11), (12), and (13), the term $J(\beta)$ in (14) is

$$J = j\frac{(a+c)^2}{2} I \tag{A1}$$

$$I = \int_0^\infty \frac{(1+\cos 2\omega)}{\sqrt{\omega^2 + p^2}} \cdot \frac{\omega^2 + \beta^2 (a+c)^2}{\left[(\pi/2)^2 - \omega^2\right]^2} d\omega \tag{A2}$$

where

$$p = (a+c)\sqrt{\beta^2 - k_0^2}, \qquad \omega = k_x (a+c). \tag{A3}$$

Although the integral in (A1) can be evaluated fairly easily by numerical means as the integrand decreases as

fast as ω^{-3}, we use an alternative procedure based on the contour integral technique. This will enable us to evaluate a part of the integral analytically. The remainder becomes an integral with an exponentially decaying integrand. Therefore, the evaluation is much less time consuming. Such a feature is important as we evaluate the integral in the iteration algorithm. To this end, we recognize

$$I = \mathrm{Re}\int_0^\infty \frac{1+e^{j2\omega}}{\sqrt{\omega^2+p^2}} \frac{\omega^2+\beta^2(a+c)^2}{\left[(\pi/2)^2-\omega^2\right]^2} d\omega. \tag{A4}$$

With this method of contour integration, (A4) can be calculated by choosing the integral path which avoids the pole at $\pi/2$ and the branch point jp as shown in Fig. 6. Since there is no singularity inside the contour, the contour integration is zero. The integral along the semi-infinite contour is zero as the integrand converges and the one around the branch jp is also zero. The integral from jp to 0 provides an imaginary value. Therefore, only the contribution around the pole and the integral from $j\infty$ to jp contribute to the evaluation of I. The following equation will be obtained:

$$J = j\frac{(a+c)^2}{2}\left\{\frac{2}{\pi}\frac{\left[(\pi/2)^2+\beta^2(a+c)^2\right]}{\sqrt{(\pi/2)^2+p^2}} + \int_p^\infty \frac{\beta^2(a+c)^2-r^2}{\sqrt{r^2-p^2}\left[(\pi/2)^2+r^2\right]^2} dr + \int_p^\infty \frac{\left[\beta^2(a+c)^2-r^2\right]e^{-2r}}{\sqrt{r^2-p^2}\left[(\pi/2)^2+r^2\right]^2} dr\right\}. \tag{A5}$$

The first integral of the above equation can be evaluated analytically [4], and the second one is computed numerically by using associated Gauss–Laguerre quadrature formulas. The final result comes out as follows:

$$J = j\frac{(a+c)^2}{2}\left\{\frac{2}{\pi}\frac{\left[(\pi/2)^2+\beta^2(a+c)^2\right]}{\sqrt{(\pi/2)^2+p^2}} + I_1 + I_2\right\} \tag{A6}$$

where

$$I_1 = \frac{1}{\pi\sqrt{(\pi/2)^2+p^2}} \cdot \left\{1+\frac{\left[(\pi/2)^2+\beta^2(a+c)^2\right](\pi^2+2p^2)}{\pi^2\left[(\pi/2)^2+p^2\right]}\right\} \cdot \ln\frac{\sqrt{(\pi/2)^2+p^2}+\pi/2}{\sqrt{(\pi/2)^2+p^2}-\pi/2} - \frac{2\left[(\pi/2)^2+\beta^2(a+c)^2\right]}{\pi^2\left[(\pi/2)^2+p^2\right]} \tag{A7}$$

$$I_2 = 4\cdot e^{-2p}\int_0^\infty \frac{e^{-x}}{\sqrt{x}} f(x)\, dx \tag{A8}$$

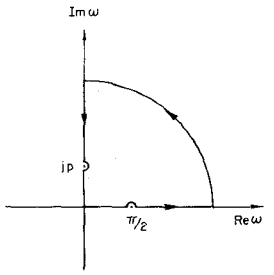

Fig. 6. Contour of integration in the ω-plane.

$$f(x) = \frac{4\beta^2(a+c)^2-(x+2p)^2}{\sqrt{x+4P}\left[\pi^2+(x+2p)^2\right]^2}. \tag{A9}$$

It should be noted that the numerical calculation of (A8) is quite efficient due to an exponential factor.

References

[1] T. Itoh and B. Adelseck, "Trapped image guide for millimeter-wave circuits," *IEEE Trans. Microwave Theory Tech.*, vol. MTT-28, pp. 1433–1436, Dec. 1980.

[2] T. Kaneki, "A comparison between the channel guide and trough guide about the phase constant," *Trans. Inst. Electron. Communication Engineers*, (in Japanese), vol. J59-B, pp. 211–213, Mar. 1976.

[3] K. Solbach, "Electric probe measurement on dielectric image lines in the frequency range of 20–90 GHz," *IEEE Trans. Microwave Theory Tech.*, vol. MTT-26, pp. 755–758, Oct. 1978.

[4] I. S. Gradshteyn and I. M. Ryzhik, *Table of Integrals, Series, and Products*. New York: Academic Press, 1965, pp. 55, 68, 89.

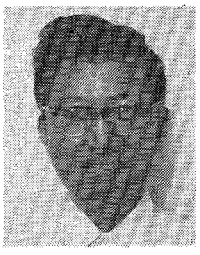

Wen-biao Zhou was born in Wuxi, Jiangsu, China, in 1939. He graduated from the Nanjing Institute of Technology, Nanjing, China, in 1961.

From 1961 to 1962 he was a Teaching Assistant in the Department of Physics, Wuhan University, Wuhan, China. In 1965, he joined the Institute of Electronics of the Chinese Academy of Sciences, Beijing, China, where he is now a Research Associate.

At present, he is a Visiting Scholar at the Department of Electrical Engineering, University of Texas at Austin.

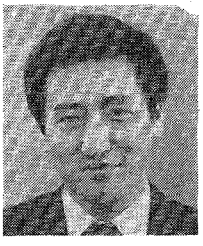

Tatsuo Itoh (S'69–M'69–SM'74–F'82) received the Ph.D. degree in electrical engineering from the University of Illinois, Urbana, in 1969.

From September 1966 to April 1976 he was with the Electrical Engineering Department, University of Illinois. From April 1976 to August 1977 he was a Senior Research Engineer in the Radio Physics Laboratory, SRI International, Menlo Park, CA. From August 1977 to June 1978 he was an Associate Professor at the University of Kentucky, Lexington. In July 1978 he joined the faculty at the University of Texas at Austin, where he is now a Professor of Electrical Engineering and Director of the Microwave Laboratory. During the summer of 1979, he was a guest researcher at AEG-Telefunken, Ulm, West Germany.

Dr. Itoh is a member of the Institute of Electronics and Communication Engineers of Japan, Sigma Xi, and Commission B of USNC/URSI. He serves on the Administrative Committee of IEEE Microwave Theory and Techniques Society. He is a Professional Engineer registered in the State of Texas.